https://doi.org/10.3311/PPci.14846

Periodica Polytechnica Civil Engineering, 64(1), pp. 81–100, 2020

Effects of Wet Separated and High Speed Milling Fly Ash Added in High Volume to Cementitious Materials

Usman Haider[1*], Asif Ali[2], Zdeněk Bittnar[1], Muhammad Humayon[3], Jan Valentin[4]

[1] Department of Mechanics, Faculty of Civil Engineering, Czech Technical University in Prague, Thákurova 7, Prague 6, 166 29, Czech Republic
[2] Department of Chemical Engineering, University of Engineering and Technology, Lahore, G.T Road, Lahore, Punjab 54890, Pakistan
[3] Parsons Transportation Group, Peachtree Corners, 3577 Parkway lane, GA 30092, USA
[4] Department of Material Engineering and Chemistry, Faculty of Civil Engineering, Czech Technical University in Prague, Thákurova 7, Prague 6, 166 29, Czech Republic
[*] Corresponding author, e-mail:

Received: 14 August 2019, Accepted: 23 September 2019, Published online: 10 January 2020

Abstract

In this research high speed milling was carried out on particles of brown coal raw fly ash, on second layer, and on third layer particles obtained from wet separation of brown coal raw fly ash. Due to milling process, median particle size d_{50} of raw fly ash, second layer, and third layer reduced by 46 %, 23 %, and 77 %, densities reduced by 11 %, 17 %, and 8 % respectively. Due to milling process, formation of agglomerations was observed, the standard deviation of the chemical composition of each element from the mean value reduced. After milling, high volume cementitious paste mixes were prepared with 60 % cement replacement. Due to the milling process the increase in compressive strength at 28 and 90 days was observed for raw fly ash is 59 % and 16 %, for second layer is 12 % and 15 %, for third layer and milled third layer is 78 % and 75 %. Flexural strength testing showed that due to the milling process the deflections at maximum loads have reduced considerably leading to brittle behavior of milled cementitious specimens. The testing for Mercury Intrusion Porosimetry showed that the cementitious specimens of third layer have maximum concentration of large capillary pores between 0.05 and 10 μm, whereas, all others have maximum concentration of medium capillary pores between 0.01 and 0.05 μm. Autogenous shrinkage of cementitious specimens was measured for first sixteen hours after mixing which showed that the second layer particles have the least shrinkage as compared to all other specimens.

Keywords

milling, raw fly ash, milled, second layer, third layer, cementitious, alumina, silicate, particles

1 Introduction

High speed milling/grinding with pin mills or disintegrator is a type of high energy milling, which involves supply of energy in large amounts in a short duration of time with high power pulses [1]. In this way the amount of energy which is supplied to a solid material is much more than in conventional mills, with almost the same input power supplied [2]. Mechano-chemical activation or simply mechanical activation occurs in solids as a result of high speed milling/grinding [3].

The development of technology in the last century with the ability to improve the properties of cementitious materials while maintaining ecological processes by the incorporation of fly ashes [4]. This is because fly ash has a reactive part in it that is the amorphous phase, which consists of silica [5]. When this fly ash is mixed with cement in the presence of water, it induces a reaction with calcium hydroxide released from the hydration of Portland cement to produce calcium-silicate hydrates (CSH) [6–8] and this reaction is well known as a pozzolanic reaction.

Several researches have been carried out on mechanical activation of fly ash by using various type of mills. Mechanical activation was carried out in a laboratory scale stirred media mill using various rotors, structural changes in milled material were detected, transformation in particle morphology, and crystal defects were determined [9]. Mechanical processes during milling/grinding mineral materials cause, along with the increase in their surface energy, increase the Gibbs energy of powders, and

Cite this article as: Haider, U., Ali, A., Bittnar, Z., Humayon, M., Valentin, J. "Effects of Wet Separated and High Speed Milling Fly Ash Added in High Volume to Cementitious Materials", Periodica Polytechnica Civil Engineering, 64(1), pp. 81–100, 2020. https://doi.org/10.3311/PPci.14846

respectively their chemical activity, which also contributes to the high adhesion strength when contacting the milled material with binders [10]. Decrease in crystal state, gross distortion and enhanced reactivity of fly ash occurred due to vibratory ring mechanical milling, whereas enhanced reactivity is less prominent for planetary and conventional ball mills [11]. Fly ash milling was found to improve particle fineness, to increase the silica and alumina content in the cement, milled fly ash blended cements show higher compressive strength compared to un-milled fly ash blended cements, due to improved fly ash reactivity through their mechanical activation [12]. Higher pozzolanic activity for fly ash was achieved for the same specific surface area using high-speed pin mill with two counter rotors, and this type of mill can be a promising means of improving its properties via grinding and mechanical activation [13].

Finer and amorphous materials accelerate the pozzolanic reaction and improves characteristics of cementitious materials [14]. Efforts are being made to reduce the particle size of fly ash by several techniques/methods other than mechanical milling such as air classification systems or dry separation [15]. But air classification systems have drawbacks such as significant amount of underflow/coarse products are produced, yield of overflow/fine products produced is very low, and the cost of air classification machines is considerably high. [16–18] Wet separation of fly ashes is another method achieved to improve the size of fly ash particles. ASTM Class C fly ashes [19] if added to water reacts and rapidly hardens, however this phenomenon is rare in case of Class F fly ashes [20]. Therefore, ASTM Class F fly ashes can be mixed in water and consequently separation of its particles based on their densities relative to water can be carried out [21].

The strength and durability of cementitious structures are important as they define the service life of the structure but cracking of concrete due to shrinkage effects durability [22]. The part of shrinkage that does not include any change in volume due to ingress or loss of substances, variation of temperature, external force application and restraint could be called as autogenous shrinkage [23]. Usually early-stage autogenous shrinkage occurs within the first 24 hours after mixing with water [23]. The cementitious matrix is more prone to cracking during the first 12 hours after casting [24].

Any cementitious material having fly ash content more than 50 percent by mass of the total cementitious material is considered high volume fly ash cementitious material [25]. The main disadvantages of using high volume fly ash cementitious materials are its slow hydration reaction compared with that of cement, its longer curing time, and lower early-age strength [26]. The use of high volume fly ash in cementitious materials is highly beneficial with respect to cost, energy efficiency, and environmental benefits, making high volume fly ash cementitious materials environmentally sustainable [27].

For brown coal ASTM Class F fly ashes research was carried out by the authors on different type of morphological particles separated by wet separation and its effects on mechanical strength when added in large volumes in cementitious materials [21]. But it is still to be determined how wet separated ASTM Class F brown coal fly ash particles would behave in high volume cementitious materials when milled/grinded by high speed milling with two counter rotors.

Due to drawbacks of fly ash separation by air classifiers and conventional ball mills it necessitates the development of new techniques for separating and milling fly ash particle to increase its utilization. The purpose of this research is to carry out high speed milling using counter rotors followed by wet separation of ASTM Class F brown coal fly ash using water and then to examine the physical, morphological, and chemical properties of the milled wet separated parts of raw fly ash. After determining these properties of milled wet separated parts of raw fly ash, further aim is to determine the potential of using the milled wet separated particles of raw fly ash in high volume cementitious pastes to determine the effects on the mechanical properties, porosity, and autogenous shrinkage.

2 Materials and methods

2.1 Wet separation and high speed milling

Wet separation of ASTM Class F brown coal raw fly ash from Počerady power plant of Czech Republic was carried out as explained in [21] and [28] by the authors as shown in Fig. 1 (a) and (b). On raw fly ash and wet separated parts of raw fly ash, high speed milling was carried out by the company FF Servis spol. sro. [29] which conducts research on high-speed/high-energy milling of various materials since 2004.

The research by this organization focuses on grinding modes to optimize the milling of specific materials and ultimately testing high-speed grinding using extreme energies for selected types of materials. The high speed milling for fly ash research was carried out in this organization's innovation center. This center is equipped with a laboratory high-speed mill/disintegrator with a capacity of approximately

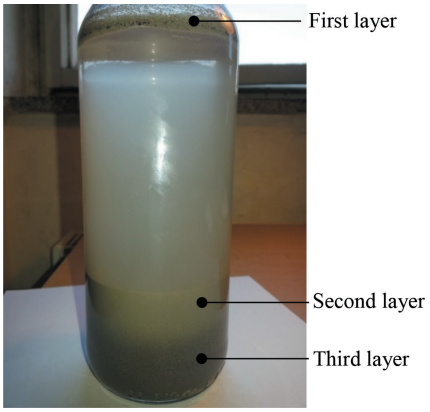

(a) [21, 28]

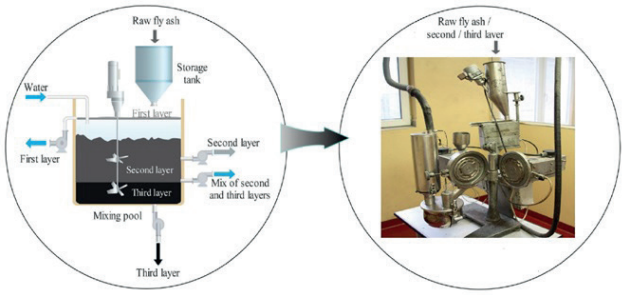

(b) [28] (c) [29, 30]

(d) [29, 30]

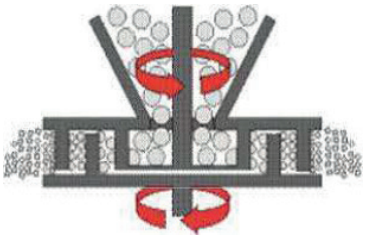

(e) [29, 30]

Fig. 1 (a) Results of mixing brown coal fly ash with water, (b) process of recovering fractions of brown fly ash by wet separation, (c) High speed milling, (d) High speed milling machine wheels, (e) high speed milling function

10–20 kg of test material per hour. The innovation center also has a processing mill for milling up to one ton of material per hour at a rotor speed of 300 m/s [30]. The high speed mill/disintegrator with counter-rotating wheels as shown in Fig. 1 (c) and (d) used in this research are specifically developed for the production of fine materials. In this research, the time of milling was kept the same for all specimens tested. Both wheels are controlled separately and can be equipped with different types of pins. One specific set of wheels were used for raw fly ash and its wet separated parts specimens. The material was fed by a continuous feeder and entered the grinding chamber through the centre of the left rotor. Only CR rotors manufactured designed and manufactured by FF Servis spol. Sro were used for all the samples. CR rotors have teeth on the left-side rotor and on the right-side rotor. The samples were prepared with two passes through the high speed milling machine/disintegrator. The particles stayed in the chamber of the high speed mill/disintegrator for only some seconds, due to the principle by which mills operate. Therefore, for extending the milling time, repeating the passes of the material again through the high speed mill is the only possible way. With the high relative velocity of the rotor blades raw fly ash and its wet separated parts were milled. In the working chamber intense collisions of fly ash particles occurred with each other, similar to those in vortex or jet mills as shown in Fig. 1 (e), this action created shock waves and cavitation effects on the surface of fly ash particles. During shock, pressure changed i.e. compression and fast expansion occurred, as a result raw fly ash and its wet separated particles were milled.

2.2 Physical properties

Particle size analysis of raw fly ash, separated fly ash particles, and milled raw fly ash and its separated milled parts were carried out on Fritsch Analysette 22, laser particle size analyzer, using its wet dispersion unit, particle size analysis results were compared with cement, EN 197-1, CEM 42.5 R. Density of raw fly ash, its separated parts, and its milled specimens were determined using helium Pycnometer, Pycnomatic ATC, and density of cement was measured for comparison. For density measurements, 100 grams of powdered samples were oven dried at a temperature of 105 °C for 12 hours to ensure the removal of moisture from the samples. Specific surface area of raw fly ash and its separated parts was measured using BET method on PC-controlled volumetric gas-adsorption system Sorptomatic 1990.

2.3 FE-SEM, EDX analyses

Microscopic images were captured on Merlin Carl Zeiss (Germany) field emission electron microscope (FE-SEM) operated at an acceleration voltage of 30 kV by HE-SE detector, under high vacuum conditions to determine morphology of raw fly ash, its wet separated particles, and its milled products. Point analyses were carried out on the images of FE-SEM by EDX software AZtecEnergy from oxford instruments. Point analysis were carried out to determine chemical composition of Si, Al, Fe, Ca, Na, Mg, S, and K in the individual raw fly ash, separated, and milled fly ash particles as these elements are known to exist in significant quantities in fly ashes [31]. Samples for microscopic testing were prepared with 1:3 solution of Araldite 2020/A epoxy resin to Araldite 2020/B hardener with two drops of Xylen solution in 50 ml solution of 1:3 epoxy to hardener ratio. The epoxy mixture added with specimens were heated to 40 °C for 2 min to give mixture a lower viscosity, thereby ensuring thorough penetration into the pores of the specimen. Then to remove air bubbles from the samples, they were vacuum impregnated at 0.17 bar pressure for 2 hours in Struers Citovac vacuum impregnation machine. After impregnation, specimens were left for hardening at a temperature of 40 °C for 24 hours. Specimens were then cut to the required shape and were diamond polished on Struers, Tegramin-25. Following the polishing to avoid charging of the specimens under electron beam of field emission scanning electron microscope, specimens were carbon coated to a thickness of 12.8 nm with Quorum Q150R ES pumped sputter carbon coater.

2.4 Cementitious paste specimens

2.4.1 Specimens for mechanical tests

Specimens of size 40 × 40 × 160 were prepared for flexural strength testing in accordance with ČSN ISO 4013 [32] with cement replacement of up to 60 % by weight with raw fly ash, second layer, third layer, milled raw fly ash, milled second layer, and milled third layer particles at w/c ratio of 0.4. For compression testing, half broken specimens from flexure test in accordance with ČSN ISO 1920 [33] were used. Mixing was carried in compliance with EN 480-1 and after preparation specimens were cured in environmental chamber at a constant temperature of 22 °C with relative humidity of 50 %. Specimens were taken from the environmental chamber for flexural and compressive strength tests which were carried out at 28 and 90 days cured specimens. During flexural testing, load and deflection of the specimens were measured for specimens cured at 90 days testing for plotting load-deflection diagram.

2.4.2 Mercury intrusion porosimetry and autogenous shrinkage measurements

Mercury intrusion porosimetry tests were carried out using Pascal 440 Porosimeter manufactured by Thermo scientific, USA to determine porosity of cementitious samples of raw fly ash, second layer, third layer, milled raw fly ash, milled second layer, and milled third layer replaced with cement. Autogenous shrinkage was measured using rubber wavy molds of height 160 mm, diameter 70 mm, and vertical deformation was measured using contactless optical deformation measuring sensors as shown in Fig. 17 (a). Cementitious specimens were prepared for raw fly ash, second layer, third layer, raw fly ash milled, second layer milled, and third layer milled specimens prepared with 60 % cement replacement having w/c of 0.4. Freshly prepared cementitious raw fly ash, second layer, third layer, milled raw fly ash, milled second layer, and milled third layer specimens were placed in environmental chamber at a constant temperature of 22 °C, with relative humidity of 50 %, and then shrinkage measurements were carried out for first 16 hours after mixing.

3 Results and discussion

3.1 Physical properties

The particle size of the materials influences quality and performance of the product, and therefore require quality control by particle characterization [34]. For this purpose, particle size distribution was carried out to find out the measures of central tendency as shown in Table 1 for Fig. 2. Median diameter, d_{50} is the size in microns that splits the distribution with half above and half below this diameter [35]. Table 1 shows that shows that cement, milled second layer, milled raw fly ash, second layer, milled third layer, raw fly ash, and third layer particles have median diameter d_{50} of 14.57, 23.26, 27.67, 30.06, 33.48, 51.07, and 146.67 μm in ascending order. This shows that milling reduced the particle size of original fed products of raw fly ash, second layer, and third layer. Median particle size d_{50} of raw fly ash was reduced by 46 %, for second layer by 23 %, and greatest reduction is observed for third layer by 77 % after milling. Upper limit diameter, d_{97} is usually used to indicate the coarse end of the powder particle size index, which is an important indicator of powder production and application [36]. Table 1 also shows that

Table 1 Physical properties

Physical properties	Cement	Raw fly ash	Milled raw fly ash	Second layer	Milled second layer	Third layer	Milled third layer
Density (g/cm^3)	3.15	2.21	2.45	1.98	2.31	2.42	2.62
Specific surface area (cm^2/g)	22000	19000	32000	38000	54000	9000	48000
Median Diameter, d_{50} (µm)	14.57	51.07	27.67	30.06	23.26	146.67	33.48
97th Percentile Diameter, d_{97} (µm)	46.96	178.94	97.85	116.32	89.49	413.29	149.48

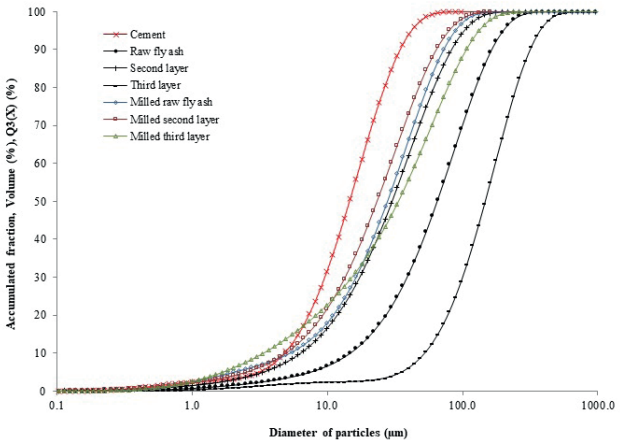

Fig. 2 Cumulative particle size distribution for particles of cement, raw fly ash, second layer, third layer, milled raw fly ash, milled second layer, and milled third layer

cement, milled second layer, milled raw fly ash, second layer, milled third layer, raw fly ash, and third layer particles have upper limit diameter d_{97} of 46.96, 89.49, 97.85, 116.32, 149.48, 178.94, and 413.29 µm in ascending order. On the similar pattern, d_{97} of raw fly ash was reduced by 45 %, for second layer by 23 %, and greatest reduction is observed for third layer by 64 % after milling. The highest reduction of particle size is observed for third layer particles because the original particle size of third layer particles is much larger as compared to the second layer or the raw fly ash particles. This shows that milling has reduced the size of larger particles considerably as compared to the smaller particles.

Comparison of densities is also presented in Table 1. Densities in ascending order for second layer, raw fly ash, milled second layer, third layer, milled raw fly ash, milled third layer, and cement are 1.98, 2.21, 2.31, 2.42, 2.45, 2.62, 3.15 g/cm^3. This shows that milling process has increased the densities of all the milled products. The difference of increase of densities after milling process for raw fly ash is 11 %, for second layer is 17 %, for third layer is 8 %. This result indicates that small particles of second layer after milling have packed up more closely together resulting in more difference of densities as compared to raw fly ash and third layer particles. Whereas, third layer particles individually being the densest particles, haven't packed up closely together as compared to second layer particles. Comparison of specific surface areas is also presented in Table 1. Specific surface areas for third layer, raw fly ash, cement, milled raw fly ash, second layer, milled third layer, and second layer are 9000, 19000, 22000, 32000, 38000, 48000, and 54000 cm^2/g. The difference of increase of specific surface areas after milling process for raw fly ash is 68 %, for second layer is 42 %, for third layer is 433 %. This result shows that specific surface area of third layer particles has increased considerably as compared to others which shows that milling process is very efficient in reducing the larger size particles as compared to smaller ones.

3.2 Morphological properties

Particle size is typically reported in units of equivalent spherical diameter owing to the ambiguity of defining the diameter of non-spherical particles and limitations intrinsic in the instrument detection system [37]. Therefore, the realistic particle morphology can be determined from electron microscopic examination of particles at different magnifications.

3.2.1 Morphological properties of separated and milled fly ash particles:

Electron microscopic images at different magnifications were observed for raw fly ash, milled raw fly ash, second layer, milled second layer, third layer, and milled third layer as shown in Fig. 3. In raw fly ash FE-SEM image of Fig. 3 (a), it is observed that raw fly ash consists of several type of particles including glassy hollow spherical, solid spherical, porous spherical, porous slaggy, compact slaggy particles, and some brighter particles as observed by the authors in [21]. However, in Fig. 3 (b) it can be seen that particles of raw fly ash are milled to a smaller size and seems distinct from each other but to determine the agglomeration of particles pseudo colored images were prepared.

Fig. 4 shows pseudo colored images as framed by the authors in [31] using software Faze based on C++ computer language in it Pseudo-colored images are transformed from the grey FE-SEM images. In these images, blue color represents the solution of the hardener and epoxy resin that was used in preparing the samples, green color represents the alumino-silicate glassy calcite regions, purple color represents the alumino-silicate glassy metallic regions, red color represents the high ferro-metallic regions, and white color represents the pure ferro metallic regions.

Fig. 4 (b) shows that due to the milling process, individual particles have agglomerated with each other. Alumino-silicate glassy calcitic particles can be seen separate from alumino-silicate glassy metallic regions in Fig. 4 (a), whereas in Fig. 4 (b) calcitic and metallic particles have agglomerated with each other.

Fig. 3 (c) and Fig. 4 (c) shows second layer which consist of majority of submicron and ultrafine (<1μm) particles with few large slaggy and porous spherical particles. The origin of these porous particles of second layer takes place when brown coal is combusted in the boiler at temperatures between 1200–1500 °C, then coal is

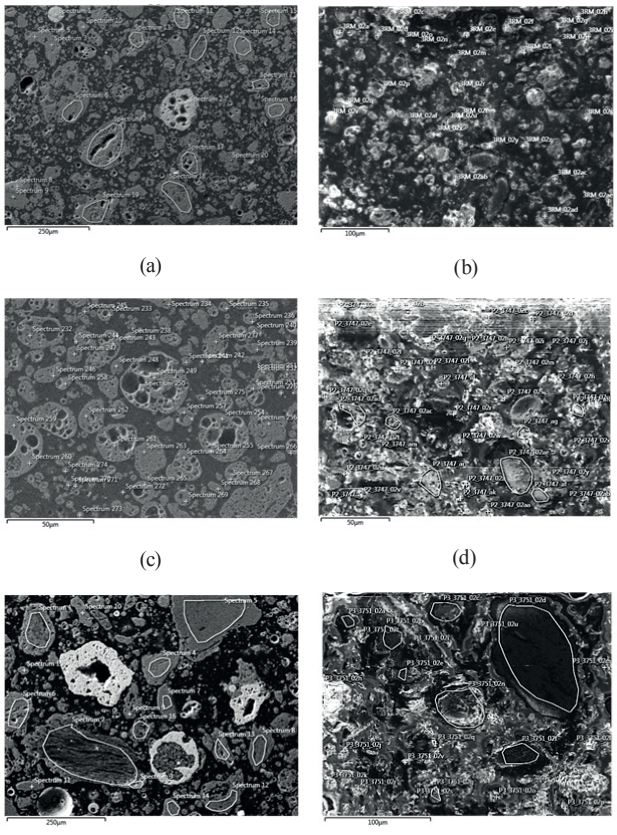

(a) (b)

(c) (d)

(e) (f)

Fig. 3 (a) Raw fly ash, (b) milled raw fly ash, (c) second layer, (d) milled second layer, (e) third layer, (f) and milled third layer

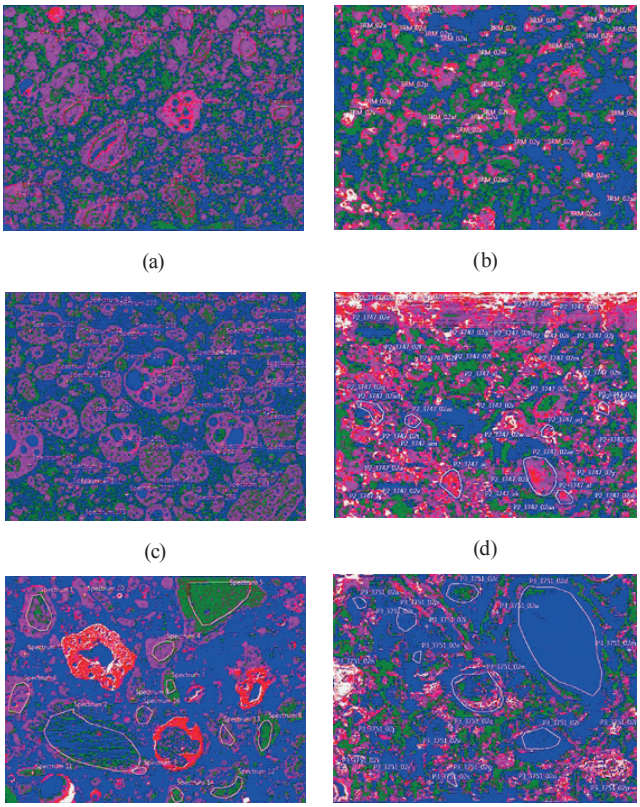

(a) (b)

(c) (d)

(e) (f)

Fig. 4 (a) Pseudo colored images for raw fly ash, (b) milled raw fly ash, (c) second layer, (d) milled second layer, (e) third layer, (f) milled third layer

spontaneously combusted and absorbed water is released from the pores of these particles to produce porous particles [21]. Fig. 3 (d) shows that the porous spherical morphology of second layer particles is broken down during the milling process. Fig. 4 (d) also shows that second layer particle morphology has broken down during milling and agglomerates have formed with enhanced alumino-silicate glassy metallic regions during milling process.

Fig. 3 (e) and Fig. 4 (e) shows FE-SEM images of third layer particles which are more compact, less porous and much bigger in size as compared to those of second layer particles and contain significant amount of bright particles [21]. In Fig. 3 (f) it can be seen that particles of third layer during milling have broken down into much smaller particles.

Fig. 4 (f) shows that particles morphology of third layer particles has broken down into much finer particles and agglomerates have formed with mixed morphology and a clear particles distinction cannot be made. Moreover, pure ferro-metallic particles or ferro-spheres present in large amount in third layer particles have broken down and have agglomerated with glassy particles.

3.2.2 Morphological properties of cementitious specimens:

Electron microscopic images at different magnifications were observed for hardened pure cement paste, hardened cement paste replaced with 60 %: raw fly ash, milled raw fly ash, second layer, milled second layer, third layer, and milled third layer samples all cured for 28 days as shown in Fig. 5. Whereas, Fig. 6 shows pseudo colored images, in them, blue color represents the solution of the hardener and epoxy resin that was used in preparing the samples, green color represents the hydration products which comprises mainly of Calcium-Silicate-Hydrate (CSH), purple color represents Portlandite (Calcium hydroxide), red color represents the unreacted cement particles such as Alite (Tri-Calcium Silicate) and Belite (Di-Calcium Silicate) primarily, and white color represents the glassy-alumino silicates mainly from fly ash particles.

The faze software used for transforming grey color microscopic images to pseudo colored images only uses five colors for phase separation, if more colors were available in the software some other small phases could also be identified which are known to be present in the hydrated cementitious mixes.

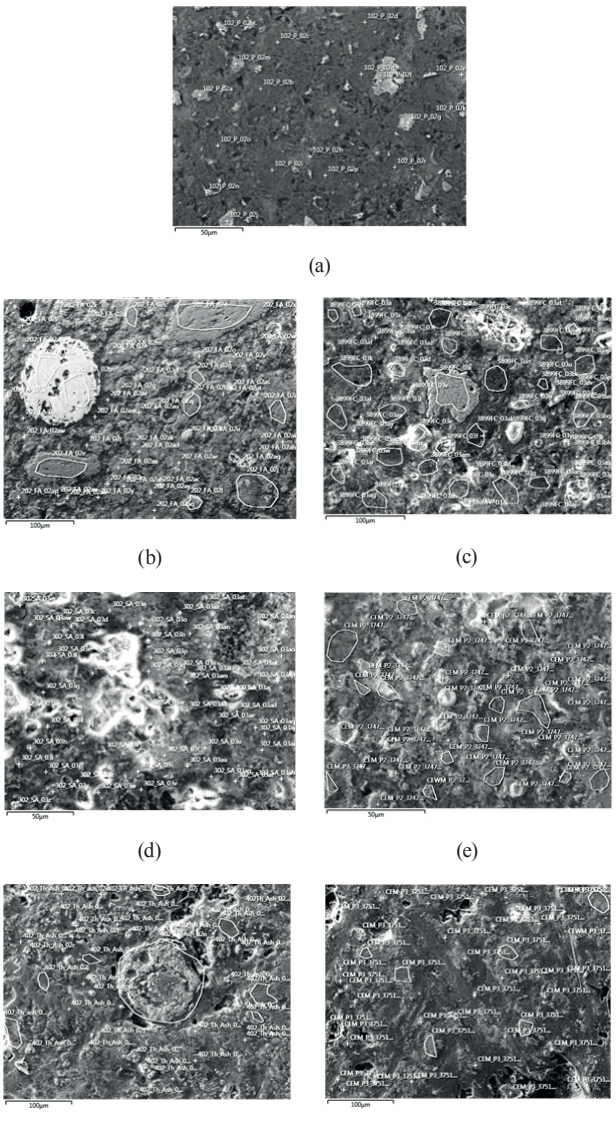

(a) (b) (c) (d) (e) (f) (g)

Fig. 5 (a) Hardened: pure cement paste, (b) cement paste with 60 % raw fly ash, (c) cement paste with 60 % milled raw fly ash, (d) cement paste with 60 % second layer, (e) Hardened cement paste with 60 % milled second layer, (f) cement paste with 60 % third layer, (g) cement paste with 60 % milled third layer

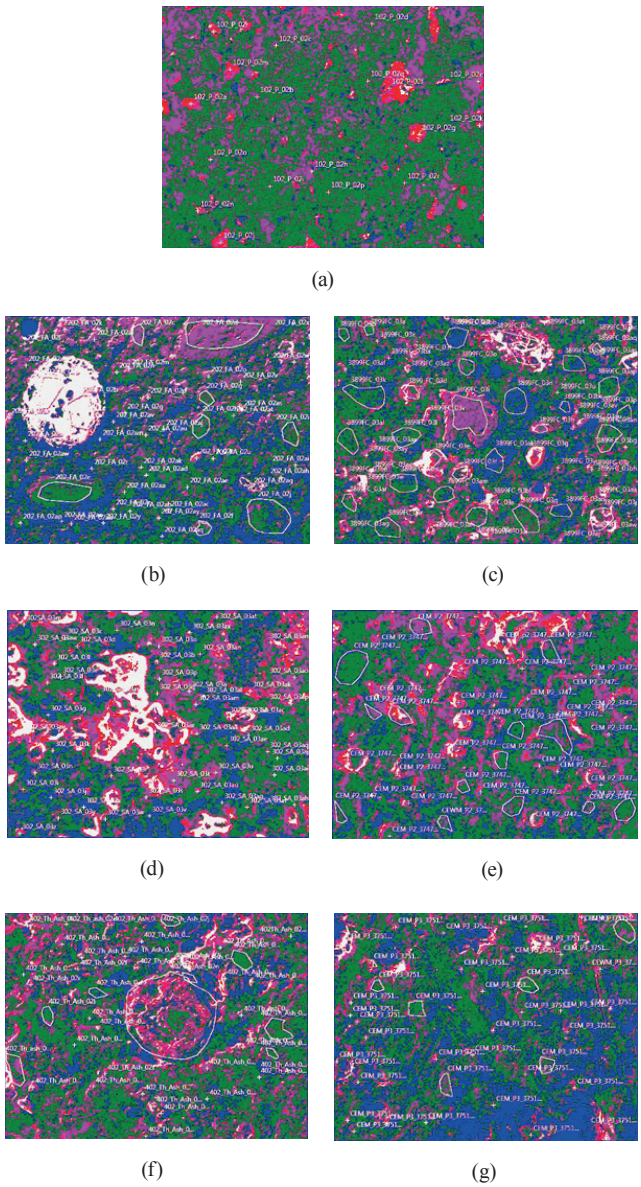

(a) (b) (c) (d) (e) (f) (g)

Fig. 6 (a) Pseudo colored images for hardened: pure cement paste, (b) cement paste with 60 % raw fly ash, (c) cement paste with 60 % milled raw fly ash, (d) cement paste with 60 % second layer, (e) cement paste with 60 % milled second layer, (f) cement paste with 60 % third layer, (g) cement paste with 60 % milled third layer

Fig. 5 (a) and Fig. 6 (a) shows grey microscopic image and transformed pseudo colored microscopic image of hardened hydrated pure cement paste.

Fig. 5 (a) combined with Fig. 6 (a) shows that hardened hydrated pure cement paste contains regions of Calcium Silicate Hydrate (CSH) gel in green color, Portlandite or Calcium hydroxide (CH) in purple color, and small regions of unreacted cement particles of Alite and Belite in red color. Calcium Silicate Hydroxide (CSH) gel has been observed by [38–40] along with Portlandite as two main phases of cement hydration process. The CSH gel occupies at least 50 % of the hardened hydrated cement paste volume [38] and it forms a continuous layer that binds together the original cement particles into a cohesive whole [38]. Calcium hydroxide or Portlandite forms as crystals with a wide range of shapes and sizes and it occupies up to 25 % of the volume of a hardened hydrated cement paste [39].

Fig. 5 (b) and Fig. 6 (b) shows grey and transformed pseudo colored microscopic images for hardened hydrated 60 % raw fly ash replaced with cement. Fig. 6 (b) show that some fly ash particles in white color are still not hydrated, the green color shows the formation of additional CSH gel when Silica from fly ash reacted with Portlandite from cement hydration. While, purple color shows the presence of Portlandite still available in the hardened paste and very small patches of red color represents the un-hydrated particles of cement such as Alite and Belite. Similar findings of hydration reaction of fly ash with cement by microscopic images has been made by [41] which states that the hardened cement – fly ash matrix consists mainly of sparse C-S-H phase, fly ash particles embedded in the matrix, and Portlandite.

Fig. 5 (c) and Fig. 6 (c) shows grey and transformed pseudo colored microscopic images for hardened hydrated 60 % milled raw fly ash replaced with cement. It can be seen in these figures that particles of raw fly ash have broken down into smaller particles and agglomeration has formed. Fig. 6 (b) shows glassy fly ash particles in spherical shape in white color. However, for comparison in Fig. 6 (c) the white color glassy particles can be seen to be agglomerated to various other particles while their original spherical shape has broken down. The milling process reduces the fraction of spherical grains, where rupture increases the specific area and, consequently, increases the reactivity of the material [42]. Moreover, cement hydrate and ground/milled fly ash particles took part in pozzolanic reaction to generate a new hydrated substance at fly ash interfaces [43].

Fig. 5 (d) and Fig. 6 (d) shows grey and transformed pseudo colored microscopic images for hardened hydrated 60 % second layer replaced with cement. It can be seen in these figures that porous spherical particles of second layer seen in Fig. 3 (c) and Fig. 4 (c) have reacted with cement to form a relatively porous matrix showing the presence of particles in white color which are still not hydrated, the green color shows the formation of additional CSH gel, purple color shows the presence of Portlandite, red color represents the un-hydrated particles of cement. Blue color of the epoxy resin and hardener can be seen within all other colors which shows that porous particles of second layer have formed a porous matrix.

Fig. 5 (e) and Fig. 6 (e) shows grey and transformed pseudo colored microscopic images for hardened hydrated 60 % milled second layer replaced with cement. These figures compared with Fig. 5 (d) and Fig. 6 (d) shows that porosity of cementitious matrix has reduced considerably when milled second layer particles are used and a nearly dense cementitious matrix is formed with little porosity. This is evident from seeing Fig. 5 (e) and Fig. 6 (e) in which it can be seen that reduction of blue color and increase of green color of CSH Gel has occurred due to milling of second layer particles as also observed by [44] when milled fly ash particles are used in cementitious pastes.

Fig. 5 (f) and Fig. 6 (f) shows grey and transformed pseudo colored microscopic images for hardened hydrated 60 % third layer replaced with cement and Fig. 5 (g), Fig. 6 (g) shows grey and transformed pseudo colored microscopic images for hardened hydrated 60 % milled third layer particles replaced with cement. Comparing Fig. 5 (f) with Fig. 5 (g) it can be seen that hardened cementitious matrix prepared with milled third layer particles of Fig. 5 (g) is denser as compared to Fig. 5 (f). However, both the pseudo colored images reveal that the cementitious matrices contains large size pores which is due to presence of large size particles of third layer and absence of particles which could fill up the voids in the large size pores.

3.3 Chemical properties

3.3.1 Box and whisker plots

Using EDX analyses, individual particles in raw fly ash of Fig. 3 were analyzed with small area and point analyses for the composition of Na, Mg, Al, Si, S, K, Ca, Ti, and Fe present in them. Fig. 7 (a)–(f) shows the box and whisker plots for percentages of these element present in the raw fly ash, milled raw fly ash, second layer, milled second layer, third layer, and milled third layer. Moreover, these box and

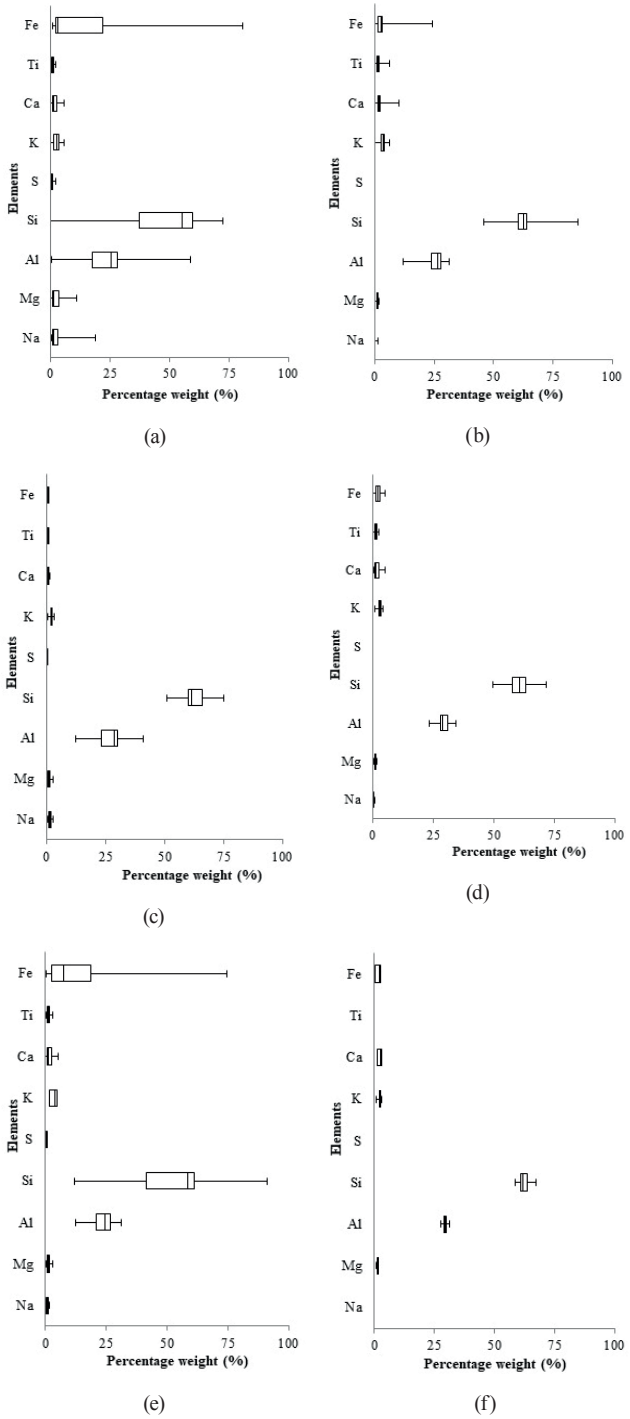

Fig. 7 (a) Box and whisker plots for raw fly ash, (b) milled raw fly ash, (c) second layer, (d) milled second layer, (e) third layer, (f) milled third layer

whisker plots show the minimum, lower quartile, median, upper quartile, and the maximum values of percentage of data of these nine elements present in the specimens.

It can be seen here clearly from box and whiskers plots that the percentages of elements in the milled samples have very less variations from the mean value, whereas un-milled samples of raw fly ash, second layer, and third layer shows that each element has scattered set of data and have large range of values. To further elaborate this aspect, Fig. 8 was prepared with the standard deviations of each element of Fig. 7 for raw fly ash, milled raw fly ash, second layer, milled second layer, third layer, and milled third layer. In Fig. 8 it can be observed that for each element, milling process has reduced the scattering of data and lesser standard deviation values are observed for milled samples. This shows that milling process influences the chemical composition of the milled end product. From the mean values of box and whisker plots of each element for raw fly ash, milled raw fly ash, second layer, milled second layer, third layer, and milled third layer were taken to prepare Fig. 9 as prepared by [45]. It can be seen from Fig. 9 that raw fly ash and third layer coarser particles have slightly different curves from all other samples. This shows that milling has influenced the mean chemical composition of milled products of raw fly ash and third layer more as compared to the influence of milling on mean chemical composition of second layer particles. However, milling has still reduced the standard deviations for milled second layer particles as seen in Fig. 8.

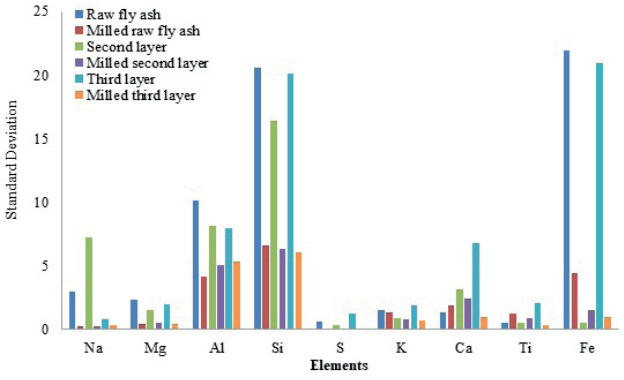

Fig. 8 Standard deviation for box and whisker plots of Fig. 7

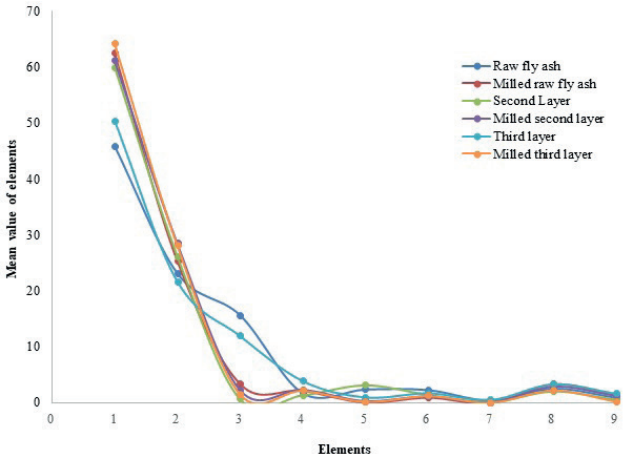

Fig. 9 Mean values of elements for box and whisker plots of Fig. 7

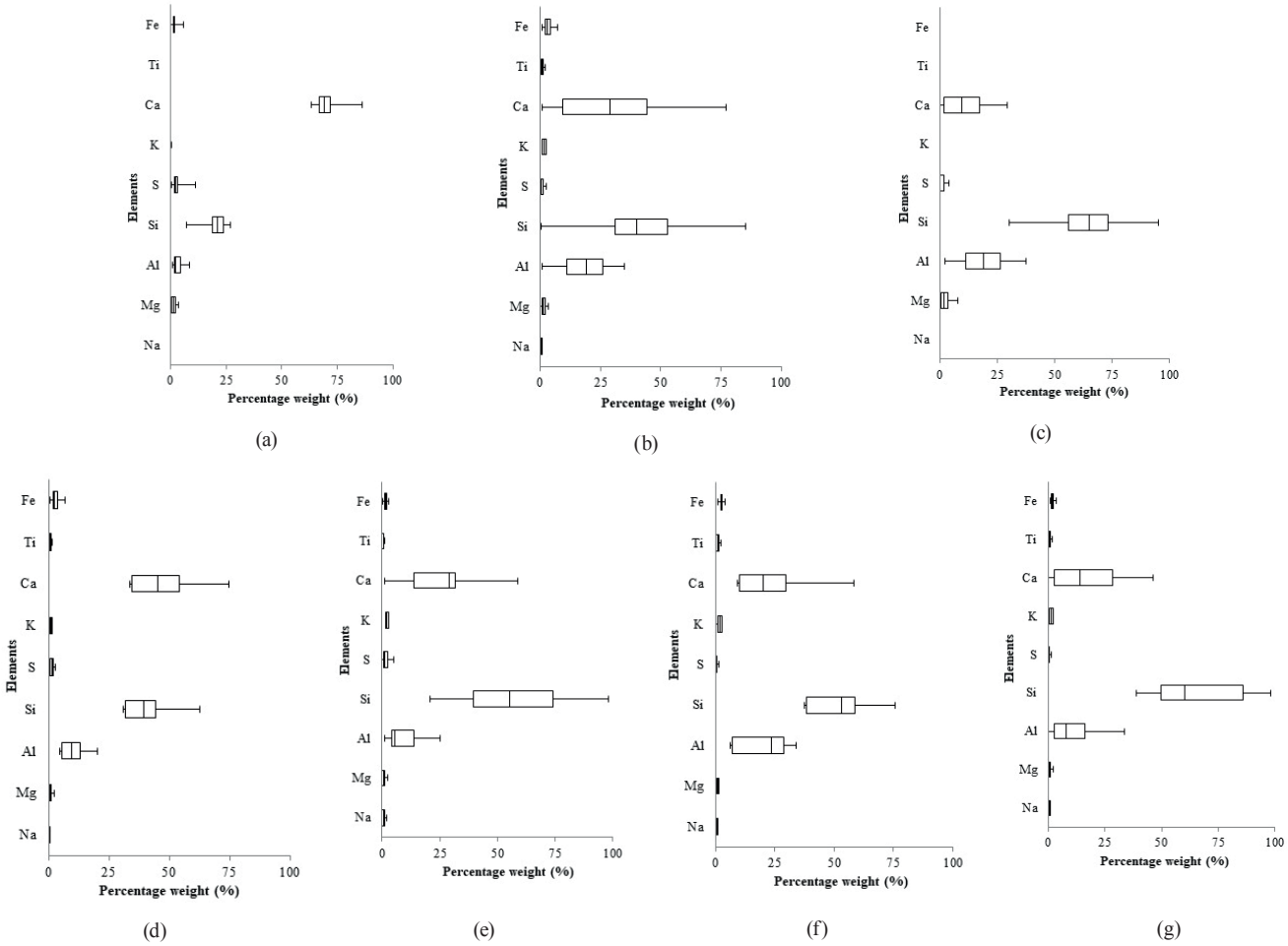

Fig. 10 (a) Hardened: pure cement paste, (b) cement paste: with 60 % raw fly ash, (c) with 60 % milled raw fly ash, (d) with 60 % second layer, (e) with 60 % milled second layer, (f) paste with 60 % third layer, (g) with 60 % milled third layer

Fig. 10 shows box and whisker plots for hardened pure cement paste, hardened cement paste with 60 %: raw fly ash, milled raw fly ash, second layer, milled second layer, third layer, and milled third layer. Fig. 10 was prepared by using EDX analyses, individual particles in cementitious mixes of Fig. 5 were analyzed with small area and point analyses for the composition of Na, Mg, Al, Si, S, K, Ca, Ti, and Fe present in them. Fig. 11 shows the mean values of elements taken from box and whisker plots of Fig. 10. Fig. 11 was prepared with slight modification to as prepared by [45], in this Ca was taken after Si, instead of after Fe as in Fig. 9. This was done because all the hardened cement paste samples had much higher contents of Ca in them due to formation of cement hydration products. Fig. 11 shows that hardened pure cement paste sample has considerably higher amount of Ca content in it. When raw fly ash is replaced with cement in hardened cement- raw fly ash sample, amount of Ca is reduced and Si and Al has increased. This shows that Si and Al has affected the overall chemical composition of hardened raw

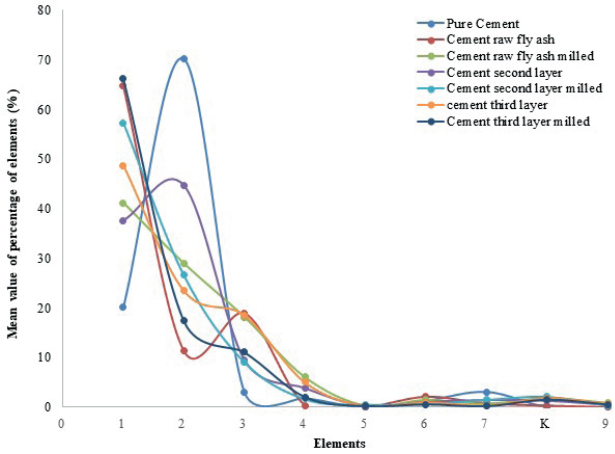

Fig. 11 Mean values of elements for box and whisker plots of Fig. 10

fly ash cementitious paste after the addition of raw fly ash. Contents of Ca also increased for hardened cement milled raw fly ash and milled third layer samples. Whereas, contents of Ca reduced for milled second layer specimens as compared to its un-milled hardened cement second layer samples. This is because milling process reduced the

particle size of raw fly ash and third layer more than second layer particles, thus for finer particles more amount of cement is used and hence Ca contents increased.

3.3.2 FE-SEM-EDX analyses plots, relationships, and ternary diagrams

Fig. 12 shows FE-SEM-EDX analyses plots of Ca vs Ca/Si for hardened pure cement paste, hardened cement paste with 60 %: raw fly ash, second layer, third layer, milled raw fly ash, milled second layer, and milled third layer. Whereas, Table 2 shows relationships from FE-SEM-EDX analyses plots of Fig. 12. It is established from Fig. 12 combined with Table 2 that for all samples, a polynomial relationship with parabolic equation $[Ca] = a[Ca/Si]^2 + b[Ca/Si] + c$, exists between Ca and Ca/Si atomic ratio with variables a, b, and c. The parabolic equations for all samples has R^2 value around 0.9 except that of hardened pure cement sample for which this relationship is very weak.

Fig. 13 was prepared for Al/Ca vs Si/Ca atomic ratios in accordance with [46–48] C-S-H was identified and is marked in dotted shape in Fig. 13. Extending the concept of [46–48] for Al/Ca vs Si/Ca atomic ratios to fly ash containing cementitious samples it is observed in Fig. 13 that except for the sample of hardened cement paste, all other samples containing particles of fly ash have atomic ratios of Al/Ca > 0.5 and Si/Ca > 1. This shows that all these samples contain higher contents of either Al or Si due to the presence of phases of Silicates, Calcium-Silicate, Calcium-Aluminum-Silicate as identified by [49] for fly ashes. In the pozzolanic reaction of the fly ash cement paste, a chemical reaction between the reactive silica from the fly ash and excess calcium hydroxide from cement hydration forms additional C-S-H gel [50]. The C-S-H formed by this pozzolanic reaction may have wider variation in composition particularly Si/Ca ratio which tends to be higher. [51] Apart from this pozzolanic reaction, fly ash in the presence of cement hydration reaction can have reaction products such as C-A-S-H gel and calcium aluminate hydrate gel due to the presence of high alumina glassy particles of fly ash [51]. Thus from Fig. 13 it can be fairly observed that C-S-H gel with high Si/Ca ratio, C-A-S-H gel, and calcium aluminate hydrate gel are present in hardened cementitious fly ash

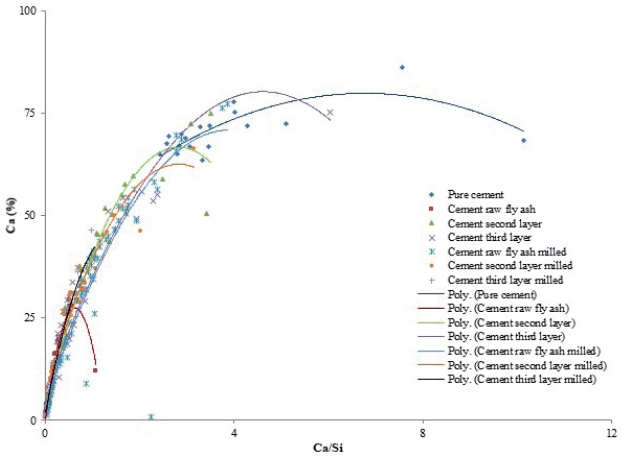

Fig. 12 FE-SEM-EDX analyses plots of Ca vs Ca/Si for hardened: pure cement paste, cement paste with: 60 % raw fly ash, with 60 % second layer, with 60 % third layer, with 60 % milled raw fly ash, with 60 % milled second layer, with 60 % milled third layer

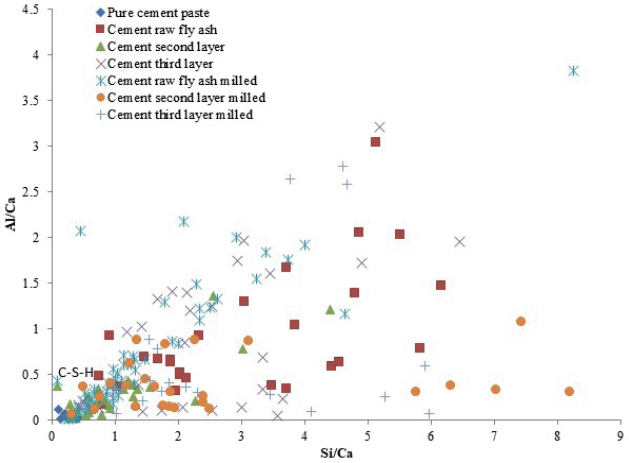

Fig. 13 FE-SEM-EDX analyses plots of Al/Ca vs Si/Ca for hardened: pure cement paste, cement paste: with 60 % raw fly ash, with 60 % second layer, with 60 % third layer, with 60 % milled raw fly ash, with 60 % milled second layer, with 60 % milled third layer

Table 2 Relationships from FE-SEM-EDX analyses plot

Sample	Relationships	R^2
Pure cement	$[Ca] = -0.8146[Ca/Si]^2 + 11.044[Ca/Si] + 42.347$	0.5843
Cement raw fly ash	$[Ca] = -69.11\ [Ca/Si]^2 + 88.197[Ca/Si] - 0.7867$	0.9784
Cement raw fly ash milled	$[Ca] = -4.3766[Ca/Si]^2 + 34.188[Ca/Si] + 4.0572$	0.8508
Cement second layer	$[Ca] = -7.9291[Ca/Si]^2 + 44.862[Ca/Si] + 3.1485$	0.9516
Cement second layer milled	$[Ca] = -6.9571[Ca/Si]^2 + 39.368[Ca/Si] + 6.7701$	0.9258
Cement third layer	$[Ca] = -3.4636[Ca/Si]^2 + 31.997[Ca/Si] + 6.2930$	0.9249
Cement third layer milled	$[Ca] = -21.110[Ca/Si]^2 + 61.267[Ca/Si] + 1.1743$	0.9632

particles paste samples. Furthermore, it can be observed from Fig. 13 that considerably lesser C-A-S-H gel and calcium aluminate hydrate gel is present in hardened cement second layer and hardened cement second layer milled specimens as compared to other hardened cementitious pastes containing fly ash particles.

Similarly, ternary diagrams are plotted in accordance with [49] as shown in Fig. 14 (a). In it red colour represents alumino-silicates, yellow colour represents calcium-silicates, blue colour represents calcium-alumino-silicates, green colour represents silicates, and grey colour represents tri-calcium silicate (alite) and di-calcium silicate (belite) [49].

The particles of raw fly ash have scattered composition, they fall mostly in red region of alumino-silicates, some in green region of silicates, very few in blue region of calcium-alumino-silicates, and some are outside all colored regions and are purely aluminates. It can be seen in Fig. 14 (b) that particles of second layer fall mostly in green silicate and red alumina-silicate colored regions, whereas third layer particles only fall in red color alumino-silicate region. In Fig. 14 (c) it can be seen that milled raw fly ash particles have composition mainly in the red alumino-silicates region with and analyses points very close to each other, which show that due to milling the scattered composition of raw fly ash has come fairly close to each other due to agglomerations. Fig. 14 (d) shows the ternary diagram for composition of second layer milled and third layer milled particles. It can be seen here that particles of second layer milled and third layer milled lies in the green silicate and red alumina-silicate regions.

Fig. 14 (e) shows ternary plot for comparison of hardened pure cement paste and hardened cementitious paste with 60 % raw fly ash. It can be seen here that the pure cement paste lies in the grey regions of tri-calcium silicate (alite) and di-calcium silicate (belite), whereas cementitious raw fly ash lies in the green silicates, yellow calcium-silicates, and red alumino-silicates regions and some in the grey regions of tri-calcium silicate (alite) and di-calcium silicate (belite). Fig. 14 (f) shows that pure cement particles lie in the grey regions of tri-calcium silicate (alite) and di-calcium silicate (belite), cement second layer lies in the area of yellow calcium-silicates, and blue calcium-alumino-silicate regions and some in the grey regions of tri-calcium silicate (alite) and di-calcium silicate (belite). Whereas, composition of cementitious third layer particles lies in the green and yellow regions.

Fig. 14 (g) shows ternary diagram for comparison of hardened pure cement paste and for hardened cementitious raw fly ash milled samples. Composition of pure

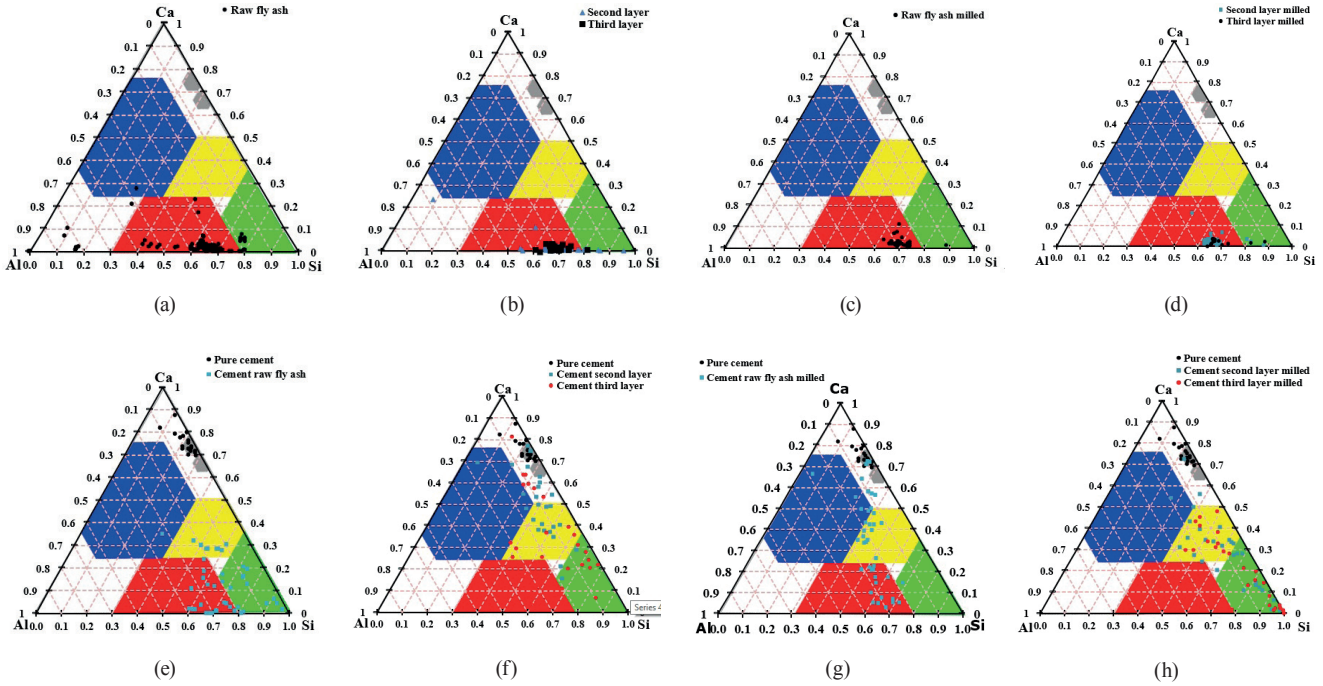

Fig. 14 (a) Ternary FE-SEM-EDX analyses diagrams for raw fly ash, (b) second layer and third layer, (c) raw fly ash milled, (d) cement second layer milled and cement third layer milled, (e) Pure cement paste and hardened cement raw fly ash, (f) pure cement paste, hardened cement second layer, and hardened cement third layer, (g) pure cement paste and cement raw fly ash milled, (h) pure cement paste, cement second layer milled, and cement third layer milled

cement paste lies in the grey regions or closer to the grey regions of tri-calcium silicate (alite) and di-calcium silicate (belite), Whereas, composition of raw fly ash milled lies in the red alumino-silicates regions, yellow calcium-silicates regions, green regions of silicates, blue regions of calcium-alumino-silicates, and grey regions of tri-calcium silicate (alite) and di-calcium silicate (belite).

Fig. 14 (h) shows the ternary diagram for comparison of pure cement paste, cementitious second layer milled, and for cementitious third layer milled samples. Composition of pure cement paste lies in the grey regions of tri-calcium silicate (alite) and di-calcium silicate (belite). It can be seen here that cementitious milled second layer samples lie in the green regions of silicates, yellow calcium-silicates regions, blue regions of calcium-alumino-silicates, and grey regions of tri-calcium silicate (alite) and di-calcium silicate (belite). Whereas, the cementitious third layer samples lie in the green regions of silicates and yellow calcium-silicates regions.

3.4 Mechanical properties

60 % cement replaced with raw fly ash, milled raw fly ash, second layer, milled second layer, third layer, and milled third layer high volume cementitious paste samples were prepared. Compressive and flexural strengths were tested at 28 and 90 days as shown in Fig. 15 (a) and (b), load vs. deflection in flexure were plotted after testing for specimens at 90 days as shown in Fig. 15 (c) for hardened cement paste with 60 % replacement of: raw fly ash, second layer, third layer, milled raw fly ash, second layer, and milled third layer.

It can be seen from Fig. 15 (a) that as the age of all cementitious paste samples increase from 28 to 90 days, the compressive strength of all the samples increase. The percentage increase between 28 and 90 days for cementitious samples of raw fly ash, second layer, third layer, raw fly ash milled, second layer milled, and third layer milled are 75, 76, 37, 28, 81, and 35 % respectively. At 28 days the percentage difference of strength comparison between raw fly ash and milled raw fly ash particles is 59 %, for second layer and second layer milled specimens is 12 %, for third layer and third layer milled specimens is 78 %. Similarly, at 90 days the percentage difference of strength comparison between raw fly ash and milled raw fly ash particles is 16 %, for second layer and second layer milled specimens is 15 %, for third layer and third layer milled specimens is 75 %. The reason for strength gain of samples as the age of specimen's increase is because of the pozzolanic

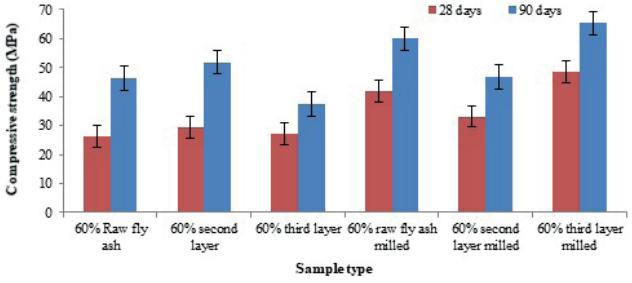

(a)

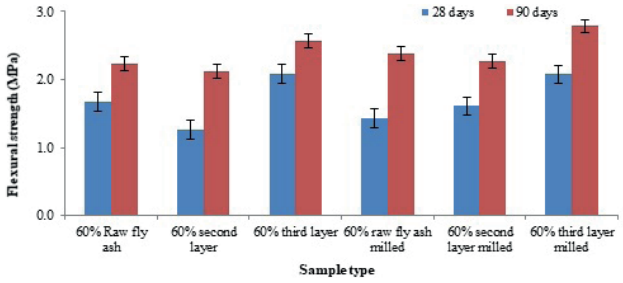

(b)

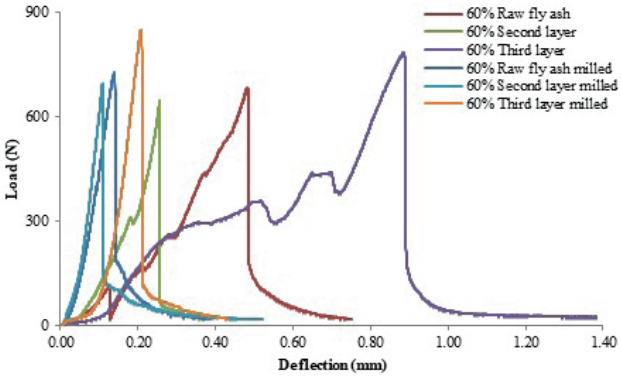

(c)

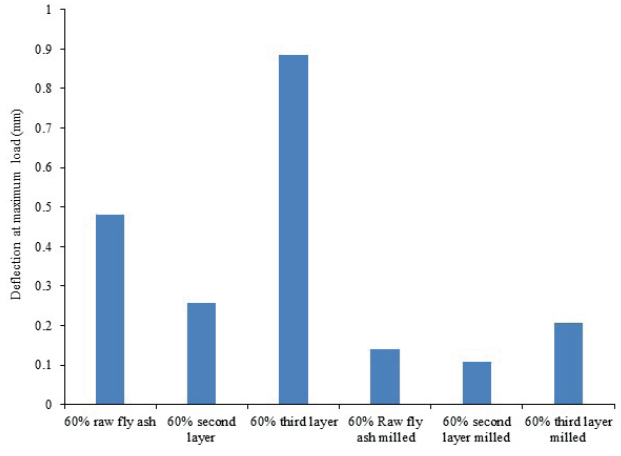

(d)

Fig. 15 (a) Comparison of compressive strengths, (b) flexural strengths, (c) load vs deflections for 90 days cured specimens, (d) deflection at maximum load charts for 90 days cured specimens for hardened cement paste: with 60 % raw fly ash, with 60 % second layer, with 60 % third layer, with 60 % milled raw fly ash, with 60 % milled second layer, with 60 % milled third layer

reaction. Pozzolanic reaction occurs when the cement particles start reacting with water they produce calcium silicate hydrates and calcium hydroxides, while silica and alumina in raw fly ash, second, third layer, milled raw fly ash, milled second layer, and milled third layer particles react with this calcium hydroxide to form additional calcium silicate hydrates and calcium aluminate hydrates which starts to give strengths mainly at and after 28 days [14, 52]. It was observed in Table 1 that due to the milling process, the median particle size d_{50} of raw fly ash was reduced by 46 %, for second layer by 23 %, and greatest reduction is observed for third layer by 77 % after milling.

Because of the reduction in particle size due to milling, the compressive strength increased. The greatest compressive strength increase due to milling is observed for third layer particles of 75 % because of highest 77 % reduction in particle size, d_{50}.

It can be seen from Fig. 15 (b) that as the age of all cementitious paste samples increase from 28 to 90 days, the flexural strength of all the samples increase. The reason for flexural strength gain of samples as the age of specimen's increase is because of the same reason that is the pozzolanic reaction. As compared to cementitious raw fly ash samples the flexural strength of cementitious third layer samples increased by 24 %. This is because of the compact angular fiber type morphology of third layer particles which resist flexural load more than spherical particles and hence show more flexural strengths. [53, 54] However, due to milling process this fiber type particle morphology of third layer particles is broken down and no significant strength increase is observed between cementitious third layer and cementitious milled third layer particles at 28 days. However, only 8 % increase of flexural strength is observed between cementitious third layer and cementitious milled third layer particles at 90 days. Fig. 15 (c) and (d) shows that the highest deflection at failure load is observed for samples with third layer particles, but due to the milling process, the deflections in flexure has reduced for all the milled specimens. The reason for lesser deflection at failure loads for milled specimens is that the angular particle morphology of brown coal fly ash particles that takes load in flexure due to better interlocking of angular particles [55] has been broken down during milling process. Thus the reduction of deflection results in more brittle behavior of the milled specimens which reduces warning before failure of a structural element at failure loads.

3.5 Mercury intrusion porosimetry

To determine the porosity in each specimen it is necessary to determine the type of pores that exist in the hydrated cementitious specimens. [21] Pores can be divided into gel pores, capillary pores, hollow-shell pores, air voids, pores in the aggregate, pores associated with interface between aggregate and cement paste, water pores, and pores due to internal discontinuities. [56] Mercury intrusion porosimetry is well known method to determine pore size distribution of specimens [21] and it is carried out to determine porosity of cementitious samples replaced with 60 %: raw fly ash, second layer, third layer, raw fly ash milled, second layer milled, and third layer milled cementitious specimens as shown in Fig. 16.

According to [57] gel pores have sizes less than 0.01 μm, medium capillary pores have sizes between 0.01 and 0.05 μm, and large capillary pores have sizes between 0.05 and 10 μm. These three types of pores are marked with vertical lines in Fig. 16 to distinguish between each type of pore. The C-S-H gel which forms by the reaction of cement in presence of water is a colloidal amorphous gel which itself contain pores of sizes less than 0.01 μm. [56] Gel pores doesn't affect the strength or water permeability of cementitious mixes and only affects shrinkage and creep. [57] Whereas, capillary pores are interconnected spaces in the hydrated cement paste between hydration products which are partially or completely filled with water. [58] Fig. 16 (a) shows cumulative pore size distribution curves between cumulative pore volume and pore diameter. Fig. 16 (b) shows differential pore size distribution curves which are obtained by differentiating the curves in Fig. 16 (a). Region under the differential curves represents the concentration of pores. [59] The peak of the differential curve corresponds to the value of critical diameter and it is the most frequently occurring pore size in interconnected pores which is one of the most important indicators of permeability. [60] In Fig. 16 (b) it can be seen that samples containing raw fly ash, second layer, third layer, raw fly ash milled, second layer milled, and third layer milled particles show the maximum concentration of pores at critical diameters with different differential peak volumes as shown in Fig. 16 (c).

It can be seen in Fig. 16 (c) that third layer particles have maximum concentration of large capillary pores, whereas raw fly ash, second layer, milled raw fly ash, milled second layer, and milled third layer samples have maximum concentration of medium capillary pores. However, second

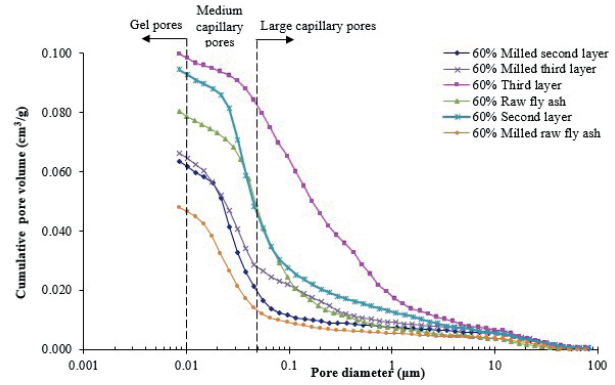

(a)

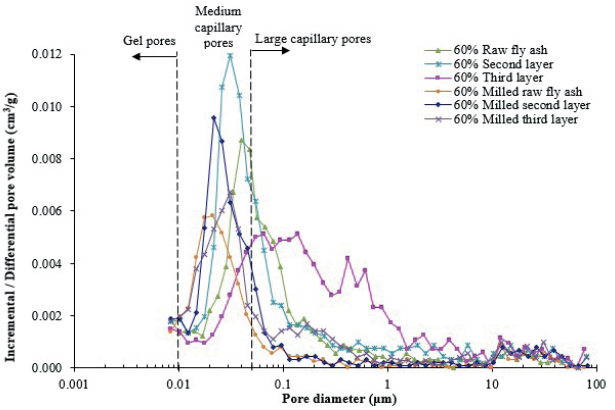

(b)

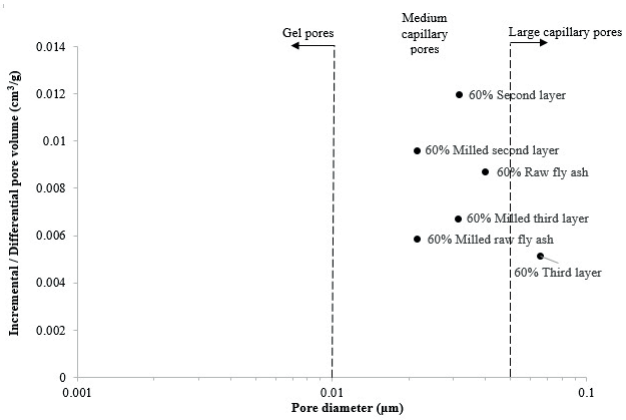

(c)

Fig. 16 (a) Comparison of cumulative pore volume vs pore diameter, (b) Incremental/Differential pore volume vs. pore diameter, (c) maximum concentration of pores at critical diameters for hardened cement paste: with 60 % raw fly ash, with 60 % second layer, with 60 % third layer, with 60 % milled raw fly ash, with 60 % milled second layer, with 60 % milled third layer

layer samples have highest concentration of these medium capillary pores because of the porous morphology of second layer particles as seen in Fig. 3 (d).

3.6 Autogenous shrinkage

Autogenous shrinkage is a macroscopic reduction in length caused by water absorption during cement hydration under constant temperature and without any moisture migration to or from the cementitious mix. [61] Therefore, autogenous shrinkage was measured under a constant temperature using improved apparatus from as used by [62] with optical sensors as shown in Fig. 17 (a). Autogenous shrinkage is explained by [63] with a four staged process in which firstly after cementitious mix is prepared, sedimentation starts and solid fraction starts to move downward under the force of gravity, the hydration process doesn't affect shrinkage in this stage. Secondly, accelerated sedimentation occurs in which hydration starts very slowly but still sedimentation continues. Thirdly, autogenous shrinkage occurs due to hydration of cement between 3 to 12 hours after mixing, in which as the cement hydrates all the cement particles become bounded by their hydrates, at this stage the water in the small capillaries exert hydrostatic tension, as a result the capillary pressure reduces the distance between the solid cementitious particles and because of it cementitious mix shrinks. Lastly, the post

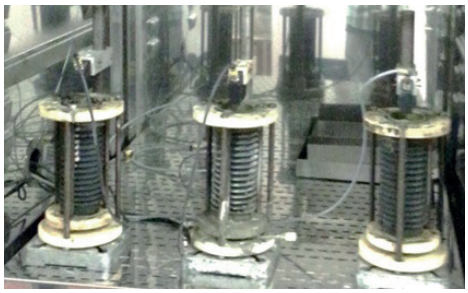

(a)

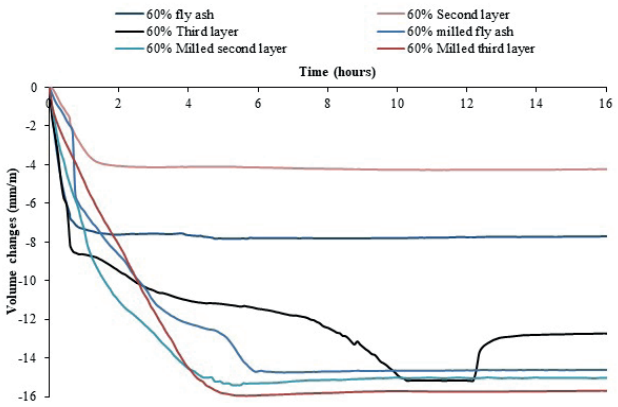

(b)

Fig. 17 (a) Autogenous shrinkage measurements apparatus, (b) volume changes vs age for: 60 % raw fly ash, 60 % second layer, 60 % third layer, 60 % milled raw fly ash, 60 % milled second layer, 60 % milled third layer replaced with cement specimens for first sixteen hours after mixing

autogenous shrinkage starts when particles in cementitious mix becomes fix to each other due to hardening of cement paste because of generation of hydration products and thus particle settlement seizes.

Fig. 17 (b) shows the volume changes for samples of cementitious mixes with 60 % of raw fly ash, second layer, third layer, raw fly ash milled, second layer milled, and third layer milled replaced with cement mixes in first sixteen hours after mixing. It can be observed from Fig. 17 (b) that specimens containing second layer particles show lesser sedimentation then specimens containing raw fly ash or third layer specimens. Reduction of sedimentation in samples containing second layer particles is due to lesser particle density of glassy, spherical and rounded, porous shape of second layer particles. As autogenous shrinkage is the result of water consumption in the hydration process, larger free water can therefore reduce shrinkage. [64] Specimens containing second layer particles retained less water than compact irregular third layer particles and this resulted in large free water content in the specimens with second layer particles cementitious mixture and hence reduction of autogenous shrinkage occurred. Also the specimens containing second layer particles retained less water because of fewer amounts of large capillary pores between 0.1 to 1 μm as seen in Fig. 16 (b) and (c). Whereas, in Fig. 17 (b) the specimens containing third layer particles show large volume change due to sedimentation. Here, significant sedimentation due to high density of compact third layer particles governs the hydration reaction and large volume change occurs over a significant length of time while the hydration continues. When sedimentation completes and third layer particles attain equilibrium, then remaining cement particles hydrate and autogenous shrinkage occurs. This happens due to high concentration of cement particles in the third layer cementitious mix as compared to others and as specimens containing irregular third layer particles retained more water due to their morphology [65] and due to large amounts of large capillary pores between 0.1 to 1 μm as seen in Fig. 16 (b) and (c). For milled raw fly ash, milled second layer, and milled third layer specimens, due to the milling process the densities of particles have increased as seen in Table 1. Thus for all the milled specimens the sedimentation and autogenous shrinkage increase.

4 Conclusions

In this research high speed mill with counter rotating wheels is used for grinding/milling the raw fly ash and wet separated parts of raw fly ash obtained from Počerady power plant of Czech Republic. Following milling, physical, chemical, and morphological properties of raw fly ash, wet separated parts of raw fly ash, and their milled particles were tested. Following this, high volume cementitious paste mixes were prepared with 60 % cement replacement of raw fly ash, wet separated particles of raw fly ash, and their milled particles. On these specimens morphological, chemical, and mechanical tests were performed including the testing for MIP and autogenous shrinkage, which leads to the following conclusions:

1. It was tested that median particle size d_{50} in ascending order of cement, milled second layer, milled raw fly ash, second layer, milled third layer, raw fly ash, and third layer particles are 14.57, 23.26, 27.67, 30.06, 33.48, 51.07, and 146.67 μm. Due to milling process, the reduction in median particle size d_{50} of raw fly ash, second layer, and third layer are 46 %, 23 %, and 77 %. Similarly, the reductions in densities for the same are 11 %, 17 %, and 8 % respectively.
2. Pseudo colored images were transformed from FE-SEM images and alumino-silicate glassy calcitic regions, alumina-silicate glassy metallic regions, high ferro-metallic regions, and pure ferro metallic regions were observed in all the specimens. Due to the milling process, formation of agglomerations was observed. Similarly, for the cementitious specimens, when pseudo colored images were transformed from FE-SEM images then Calcium Silicate Hydrate (CSH), Portlandite (CH), unreacted cement particles of Alite and Belite, and glassy alumina-silicate particles of fly ashes were observed.
3. Using EDX individual particle analyses on FE-SEM images, box and whisker plots were prepared for chemical composition of Na, Mg, Al, Si, S, K, Ca, Ti, and Fe for raw fly ash, separated particles of fly ash, and their milled particles. It was observed that due to the milling process, the standard deviation of the chemical composition of each element from the mean value had reduced. Similarly, box and whisker plots were prepared for cementitious specimens. It was observed in it that the contents of Ca have considerably increased for all the cementitious particles.
4. FE-SEM-EDX analyses plots of Ca vs Ca/Si were prepared for cementitious samples. It was found out that a strong polynomial relationship with parabolic equation $[Ca] = a[Ca/Si]^2 + b[Ca/Si] + c$ with R^2 values of 0.9 holds true for cementitious specimens containing milled and un-milled fly ashes. Whereas, this

relationship is weak for pure cement paste. When atomic ratios Al/Ca vs Si/Ca for FE-SEM-EDX analyses are plotted, calcium silicate hydrate (CSH) gel was observed for Al/Ca < 0.5 and for Si/Ca < 1. Due to the presence of fly ashes in cementitious pastes, for atomic ratios of Al/Ca < 0.5 and for Si/Ca < 1. Due to the presence of fly ashes in cementitious pastes for atomic rations of Al/Ca > 0.5 and Si/Ca > 1 phases of silicates, calcium silicates, and calcium alumina silicates were observed. This indicated the presence of hydration products of calcium aluminate hydrate (CAH) and of calcium alumina silicate hydrate (CASH) along with calcium silicate hydrate gel (CSH).

5. Ternary phase diagrams were plotted for raw fly ashes and for cementitious specimens. In it regions were distinguished from each other with different colors. Red, yellow, blue, green, and grey colors representing alumina-silicates, calcium silicates, calcium alumina silicates, silicates, and Alite and Belite. EDX analyses of raw fly ashes fall mostly in the red regions of alumina silicates and some in the blue and green regions of calcium alumina silicates and silicates respectively. Whereas, in the ternary diagrams for cementitious samples EDX analyses fall mostly in the yellow regions of calcium silicates, blue regions of calcium alumino-silicates, and in grey regions of tri calcium silicate (Alite) and di calcium silicate (Belite).
6. Percentage compressive strength difference between cementitious samples at 28 and 90 days of: raw fly ash and milled raw fly ash specimens is 59 % and 16 %, second layer and second layer milled is 12 % and 15 %, third layer and milled third layer is 78 % and 75 %. Increase in flexural strength is observed for each specimen as the age of cementitious paste increases from 28 to 90 days but no significant increase in flexural strength is observed between the raw fly ashes and their milled counter parts because the angular fibre type morphology of particles have broken down during the milling process. It is further in flexural strength testing that cementitious samples with milled fly ashes that deflections at maximum loads have reduced considerably leading to brittle behavior of milled specimens.
7. The testing for Mercury Intrusion Porosimetry showed that the cementitious specimens of third layer had maximum concentration of large capillary pores between 0.05 and 10 µm. Whereas, all other cementitious specimens of raw fly ash, raw fly ash milled, second layer, second layer milled, and third layer milled had maximum concentration of medium capillary pores between 0.01 and 0.05 µm. However, cementitious samples of second layer showed the highest concentration of medium capillary pores due to porous nature of its particles.
8. Autogenous shrinkage of cementitious specimens was measured for first sixteen hours after mixing which showed that the second layer particles showed lesser shrinkage as compared to all other specimens. Compact irregular particles of third layer cementitious mix showed considerably higher shrinkage as compared to cementitious mix of raw fly ash or second layer particles. Due to the milling process the densities and agglomerations of raw fly ash milled, second layer milled, and third layer milled cementitious specimens increased considerably and led to the increase of autogenous shrinkage for milled specimens.

Conflict of interest

The authors declare that we have no conflict of interest.

References

[1] Mucsi, G. "Mechanical activation of power station fly ash by grinding – A review", Journal of Silicate Based and Composite Materials, 68(2), pp. 56–61, 2016. https://doi.org/10.14382/epitoanyag-jsbcm.2016.10

[2] Boldyrev, V. V. "Mechanochemistry and mechanical activation of solids", Russian Chemical Reviews, 75(3), pp. 177–189, 2006. https://doi.org/10.1070/RC2006v075n03ABEH001205

[3] Baláž, P. "Mechanochemistry in Nanoscience and Minerals Engineering", Springer-Verlag, Berlin, Heidelberg, Germany, 2008.

[4] Durán-Herrera, A., Juárez, C. A., Valdez, P., Bentz, D. P. "Evaluation of sustainable high-volume fly ash concretes", Cement and Concrete Composites, 33(1), pp. 39–45, 2011. https://doi.org/10.1016/j.cemconcomp.2010.09.020

[5] Bumrongjaroen, W., Muller, I. S., Pegg, I. L. "Characterization of Glassy Phase in Fly Ash from Iowa State University", Vitreous State Laboratory The Catholic University of America, Washington, DC, USA, Rep. VSL-07R520X-1, 2007. [online] Available at: http://www.vsl.cua.edu/reports/VSL-07R520X-1.pdf [Accessed: 13 April 2018]

[6] Thomas, M. "Optimizing the Use of Fly Ash in Concrete", Portland Cement Association, pp. 1–24, 2007. [pdf] Available at: https://www.cement.org/docs/default-source/fc_concrete_technology/is548-optimizing-the-use-of-fly-ash-concrete.pdf [Accessed: 24 April 2018]

[7] Pacewska, B., Wilińska, I. "Hydration of Cement Composites Containing Large Amount of Waste Materials", Procedia Engineering, 57, pp. 53–62, 2013. https://doi.org/10.1016/j.proeng.2013.04.009

[8] Dembovska, L., Bajare, D., Pundiene, I., Vitola, L. "Effect of Pozzolanic Additives on the Strength Development of High Performance Concrete", Procedia Engineering, 172, pp. 202–210, 2017. https://doi.org/10.1016/j.proeng.2017.02.050

[9] Molnár, Z., Kristály, F., Mucsi, G. "Mechanical Activation of Deposited Brown Coal Fly Ash in Stirred Media Mill", Acta Physica Polonica A, 126(4), pp. 988–993, 2014. https://doi.org/10.12693/APhysPolA.126.988

[10] Fediuk, R. S. "Mechanical Activation of Construction Binder Materials by Various Mills", IOP Conference Series: Materials Science and Engineering, 125, Article number: 012019, 2016. https://doi.org/10.1088/1757-899X/125/1/012019

[11] Andrić, L., Aćimović-Pavlović, Z., Petrov, M., Kostović, M., Jovanović, M., Bartulović, Z. "The type of mechano-activator effect on mechanical activation of fly ash", Journal of Mining and Metallurgy, 48 A(1), pp. 13–22, 2012. [pdf] Available at: https://www.jmma.tfbor.bg.ac.rs/Volumes/2012/02.pdf [Accessed: 15 May 2018]

[12] Ez-zaki, H., Diouri, A., Maher, M., Aidi, A., Guedira, T. "Effect of mechanical activation of fly ash added to Moroccan Portland cement", MATEC Web of Conferences, 149, Article number: 01074, 2018. https://doi.org/10.1051/matecconf/201814901074

[13] Dvořák, K., Hájková, I. "The effect of high-speed grinding technology on the properties of fly ash", Materials and technology, 50(5), pp. 683–687, 2016. https://doi.org/10.17222/mit.2015.127

[14] Shaikh, F. U. A., Supit, S. W. M. "Compressive strength and durability properties of high volume fly ash (HVFA) concretes containing ultrafine fly ash (UFFA)", Construction and Building Materials, 82, pp. 192–205, 2015. https://doi.org/10.1016/j.conbuildmat.2015.02.068

[15] Metso Corporation "Metso expect results, Metso centrifugal classifier for fly ash processing", [pdf] York, PA, USA, Available at: https://www.metso.com/globalassets/saleshub/documents---episerver/centrifugal-classifier-for-fly-ash-processing-brochure-en-lr.pdf [Accessed: 29 May 2018]

[16] Gloeckner, H., Hagemeier, T., Roloff, C., Thévenin, D., Tomas, J. "Experimental Investigation on the Multistage Particle Classification in a Zigzag Air Classifier", In: Proceedings of the World Congress on Engineering, 2, 2014. [pdf] Available at: http://www.iaeng.org/publication/WCE2014/WCE2014_pp1487-1492.pdf [Accessed: 06 June 2018]

[17] Petrus, H. T. B. M., Hirajima, T., Oosako, Y., Nonaka, M., Sasaki, K., Ando, T. "Performance of dry-separation processes in the recovery of cenospheres from fly ash and their implementation in a recovery unit", International Journal of Mineral Processing, 98(1–2), pp. 15–23, 2011. https://doi.org/10.1016/j.minpro.2010.09.002

[18] Hirajima, T., Petrus, H. T. B. M., Oosako, Y., Nonaka, M., Sasaki, K., Ando, T. "Recovery of cenospheres from coal fly ash using a dry separation process: Separation estimation and potential application", International Journal of Mineral Processing, 95(1–4), pp. 18–24, 2010. https://doi.org/10.1016/j.minpro.2010.03.004

[19] ASTM C618-19 "Standard specification for coal fly ash and raw or calcined natural pozzolan for use in concrete", ASTM International, West Conshohocken, PA, USA, 2019. [online] Available at: http://www.astm.org/ [Accessed: 20 March 2019]

[20] Kolay, P. K., Bhusal, S. "Recovery of hollow spherical particles with two different densities from coal fly ash and their characterization", Fuel, 117, pp. 118–124, 2014. https://doi.org/10.1016/j.fuel.2013.09.014

[21] Haider, U., Bittnar, Z., Kopecky, L., Bittnar, P., Nemecek, J., Ali, A., Pokorny, J. "Mechanical behaviour and durability of high volume fly ash cementitious composites", Frattura ed Integrità Strutturale, 10(38), pp. 305–318, 2016. https://doi.org/10.3221/IGF-ESIS.38.41

[22] Chindaprasirt, P., Homwuttiwong, S., Sirivivatnanon, V. "Influence of fly ash fineness on strength, drying shrinkage and sulfate resistance of blended cement mortar", Cement and Concrete Research, 34(7), pp. 1087–1092, 2004. https://doi.org/10.1016/j.cemconres.2003.11.021

[23] Wu, L., Farzadnia, N., Shi, C., Zhang, Z., Wang, H. "Autogenous shrinkage of high performance concrete: A review", Construction and Building Materials, 149, pp. 62–75, 2017. https://doi.org/10.1016/j.conbuildmat.2017.05.064

[24] van Breugel, K., van Tuan, N. "Autogenous Shrinkage of HPC and Ways to Mitigate it", Key Engineering Materials, 629–630, pp. 3–20, 2015. https://doi.org/10.4028/www.scientific.net/KEM.629-630.3

[25] Crouch, L. K., Hewitt, R., Byard, B. "High Volume Fly Ash Concrete", In: 2007 World of Coal Ash (WOCA), Covington, KY, USA, 2007, pp. 1–14. [pdf] Available at: http://www.flyash.info/2007/2crouch.pdf [Accessed: 6 August 2018]

[26] Aydin, E., Arel, H. S. "Characterization of high-volume fly-ash cement pastes for sustainable construction applications", Construction and Building Materials, 157, pp. 96–107, 2017. https://doi.org/10.1016/j.conbuildmat.2017.09.089

[27] Jiang, P., Jiang, L., Zha, J., Song, Z. "Influence of temperature history on chloride diffusion in high volume fly ash concrete", Construction and Building Materials, 144, pp. 677–685, 2017. https://doi.org/10.1016/j.conbuildmat.2017.03.225

[28] Haider, U., Bittnar, Z., Kopecky, L., Humayon, C. M. "Frakcjonowanie popiołu lotnego pochodzącego ze spalania węgla brunatnego metodą mokrą i separacji magnetycznej, oraz oznaczenie właściwości fizycznych, chemicznych oraz morfologii poszczególnych frakcji. Część 1" (Classification of brown coal fly ash fractions by wet, magnetic separation methods, and determination of physical, morphological, and chemical properties of separated fractions, Part 1), 2017(3), pp. 249–259, 2017. [online] Available at: http://www.cementwapnobeton.pl/index_old.php?s=2&action=getArticle&aid=1087&t=Frakcjonowanie+popiolu+lotnego+pochodzacego+ze+spalania+wegla+brunatnego+metoda+mokra+i+separacji+magnetycznej%2C+oraz+oznacze-

nie+wlasciwosci+fizycznych%2C+chemicznych+oraz+morfologii+poszczegolnych+frakcji.+Czesc+1 [Accessed: 10 September 2018] (in Polish)

[29] FF Servis "Research and Development for processing raw materials (both food and non-food) using the innovative High Speed Grinding methods" [online] Available at: http://www.ffservis.cz/Default.aspx [Accessed: 23 September 2018]

[30] Prokšan, Z. Procházka, M., Faltus, M., Procházka, M., Valentin, J. "Využití vysokorychlostního mletí v odpadovém hospodářství" (Utilization of high-speed grinding in waste management), [pdf] Available at: http://www.odpadoveforum.cz/TVIP2017/prispevky/135.pdf [Accessed: 24 September 2018] (in Czech)

[31] Haider, U., Bittnar, Z., Kopecky, L., Šmilauer, V., Pokorny, J., Zaleska, M., Prošek, Z., Hrbek, V. "Determining the role of individual fly ash particles in influencing the variation in the overall physical, morphological, and chemical properties of fly ash", Acta Polytechnica: Journal of Advanced Engineering, 56(4), pp. 265–282, 2016. https://doi.org/10.14311/AP.2016.56.0265

[32] UNMZ "ČSN ISO 4013 (731318), Concrete: Determination of bending tensile strength of test specimens", Králové, Czech Republic, 2001. [online] Available at: http://www.technicke-normy-csn.cz/731318-csn-iso-4013_4_16500.html [Accessed: 10 September 2018] (in Czech)

[33] UNMZ "ČSN ISO 1920 (731317) Zkoušení betonu. Rozměry, mezní odchylky a použití zkušebních těles" (Concrete testing. Dimensions, tolerances and use of test specimens), Králové, Czech Republic, 1986. [online] Available at: http://www.technicke-normy-csn.cz/731317-csn-iso-1920_4_16496.html [Accessed: 15 September 2018] (in Czech)

[34] Retsch Technology GmbH "Building Materials", [online] Available at: https://www.retsch-technology.com/applications/technical-basics/particle-analysis-building-materials/ [Accessed: 09 October 2018]

[35] Horiba Scientific "Understanding and Interpreting Particle Size Distribution Calculations", [online] Available at: http://www.horiba.com/scientific/products/particle-characterization/education/general-information/data-interpretation/understanding-particle-size-distribution-calculations/ [Accessed: 10 October 2018]

[36] 9X Minerals LLC "Paint Grade Barite Powder" [online] Available at: http://www.baritepowder.com/ [Accessed: 18 October 2018]

[37] AZO Materials "The effect of particle shape on particle size measurement", [online] Available at: https://www.azom.com/article.aspx?ArticleID=11655 [Accessed: 25 October 2018]

[38] Thomas, J., Jennings, H. "A colloidal interpretation of chemical aging of the C-S-H gel and its effects on the properties of cement paste", Cement and Concrete Research, 36, pp. 30 – 38, 2006. https://doi.org/10.1016/j.cemconres.2004.10.022

[39] Jennings, H. "A model for the microstructure of calcium silicate hydrate in cement paste", Cement and Concrete Research, 30, pp. 101–116, 2000. https://doi.org/10.1016/S0008-8846(99)00209-4

[40] Hassan, M. S. "SEM-Backscattered Imaging analysis of Cementitious Composite Matrix Incorporating Mineral Admixture", Engineering and Technology Journal, 32(4), pp. 696–703, 2014. [online] Available at: https://www.iasj.net/iasj?func=fulltext&aId=102540 [Accessed: 30 November 2018]

[41] Deschner, F., Lotenbach, B., Winnefeld, F., Schwesig, P., Seufert, S., Dittrich, S., Neubauer, J. "Investigation of a model system to characterize the pozzolanic reactivity of two low Ca fly ashes and a quartz powder", In: 13. GDCh-Tagung Bauchemie, Dortmund, Germany, 2010. pp. 127–132. (in German)

[42] Vásquez Molina, D. A., Mejía Arcila, J. M., Mejía de Gutiérrez, R. "Mechanical and thermal performance of a geopolymeric and hybrid material based on fly ash", DYNA, 83(195), pp. 216–223, 2016. https://doi.org/10.15446/dyna.v83n195.50824

[43] Seo, S. K., Chu, Y. S., Shim, K. B., Jeong, J. H. "A Study on Physical Properties of Mortar Mixed with Fly-ash as Functions of Mill Types and Milling Times", Journal of the Korean Ceramic Society, 53(4), pp. 435–443, 2016. https://doi.org/10.4191/kcers.2016.53.4.435

[44] Vázquez-Rodriguez, F. J., Valadez-Ramos, J., Puente-Ornelas, R., Contreras, J. E., Arato, A., Rodríguez, E. A. "Nonferrous waste foundry sand and milling fly ash as alternative low mechanical strength materials for construction industry: effect on mortars at early ages", Revista Română de Materiale/Romanian Journal of Materials, 48(3), pp. 338–345, 2018. [online] Available at: http://solacolu.chim.upb.ro/p338-345.pdf [Accessed: 05 December 2018]

[45] Kurda, R., Silvestre, J. D., de Brito, J. "Toxicity and environmental and economic performance of fly ash and recycled concrete aggregates use in concrete: A review", Heliyon, 4(4), Article number: e00611, 2018. https://doi.org/10.1016/j.heliyon.2018.e00611

[46] Meng, B., Fontana, P., Mueller, U., Bürgisser, P. "Influence of Natural Pozzolans on the Risk of Alkali Silica Reaction", In: ACCTA - International Conference on Advances in Cement and Concrete Technology in Africa 2013, Johannesburg, South Africa, 2013, pp. 801–808.

[47] De Weerdt, K., Justnes, H., Geiker, M. R. "Changes in the phase assemblage of concrete exposed to sea water", Cement and Concrete Composites, 47, pp. 53–63, 2014. https://doi.org/10.1016/j.cemconcomp.2013.09.015

[48] Tajuelo Rodriguez, E., Richardson, I. G., Black, L., Boehm-Courjault, E., Nonat, A., Skibsted, J. "Composition, silicate anion structure and morphology of calcium silicate hydrates (C-S-H) synthesized by silica-lime reaction and by the controlled hydration of tricalcium silicate (C3S)", Advances in Applied Ceramics, 114(7), pp. 362–371, 2015. https://doi.org/10.1179/1743676115Y.0000000038

[49] Durdziński, P. T., Dunant, C. F., Haha, M. B., Scrivener, K. L. "A new quantification method based on SEM-EDS to assess fly ash composition and study the reaction of its individual components in hydrating cement paste", Cement and Concrete Research, 73, pp. 111–122, 2015. https://doi.org/10.1016/j.cemconres.2015.02.008

[50] Bui, P. T., Ogawa, Y., Nakarai, K., Kawai, K. "A study on pozzolanic reaction of fly ash cement paste activated by an injection of alkali solution", Construction and Building Materials, 94, pp. 28–34, 2015. https://doi.org/10.1016/j.conbuildmat.2015.06.046

[51] Bumrongjaroen, W., Livingston, R. A. "A Figure of Merit for Fly Ash Replacement of Portland Cement", In: 2009 World of Coal Ash (WOCA) Conference, Lexington, KY, USA, May, 4–7, 2009. https://doi.org/10.13140/2.1.3508.3521

[52] Bendapudi, S. C. K., Saha, P. "Contribution of Fly ash to the properties of Mortar and Concrete", International Journal of Earth Sciences and Engineering, 04(06), pp. 1017–1023, 2011.

[53] Mindess, S., Young, J. F. Darwin, D. "Concrete", Prentice Hall, Englewood Cliffs, NJ, USA, 2003.

[54] Delatte, N. J. "Concrete Pavement Design, Construction, and Performance", CRC Press, Taylor & Francis Group, Boca Raton, FL, USA, 2014.

[55] Chebet, F. C., Kalumba, D. "Laboratory Investigation on Re-Using Polyethylene (Plastic) Bag Waste Material for soil reinforcement in Geotechnical Engineering", Civil Engineering and Urban Planning: An International Journal (CiVEJ), 1(1), pp. 67–82, 2014. [pdf] Available at: https://airccse.com/civej/papers/1114civej06.pdf [Accessed: 17 December 2018]

[56] Aligizaki, K. K. "Pore structure of cement-based materials, testing, interpretation and requirements", Taylor & Francis, New York, NY, USA, 2005.

[56] Zhang, M. H., Islam, J. "Use of nano-silica to reduce setting time and increase early strength of concretes with high volume fly ash or slag", Construction and Building Materials, 29, pp. 573–580, 2012. https://doi.org/10.1016/j.conbuildmat.2011.11.013

[57] Caldarone, M. A. "High-Strength Concrete: A practical Guide", Taylor & Francis Group, Chicago, IL, USA, 2009.

[58] Cardoso, A. V., Oliveira, W. J., Vaz, G. J. O. "Cortical bone porosity visualization using mercury porosimetry intrusion data", Matéria, 12(4), pp. 612–617, 2007. https://doi.org/10.1590/S1517-70762007000400010

[59] de Freitas, V. P., Delgado, J. M. P. Q. "Durability of Building Materials and Components", Springer-Verlag, Berlin, Heidelberg, Germany, 2013. https://doi.org/10.1007/978-3-642-37475-3

[60] Tazawa, E., Miyazawa, S., Kasai, T. "Chemical shrinkage and autogenous shrinkage of hydrating cement paste", Cement and Concrete Research, 25(2), pp. 288–292, 1995. https://doi.org/10.1016/0008-8846(95)00011-9

[61] Nawa, T., Horita, T., Ohnuma, H. "A study on measurement system for autogenous shrinkage of cement mixes", In: Dhir, R. K., Newlands, M. D., Harrison, T. A. (eds.) Concrete Floors and Slabs, Thomas Telford, Edinburgh, Scotland, 2002, pp. 281–290, [online] Available at: https://www.icevirtuallibrary.com/doi/abs/10.1680/cfas.31760.0027 [Accessed: 21 January 2019]

[62] Termkhajornkit, P., Nawa, T., Nakai, M., Saito, T. "Effect of fly ash on autogenous shrinkage", Cement and Concrete Research, 35(3), pp. 473–482, 2005. https://doi.org/10.1016/j.cemconres.2004.07.010

[63] Tazawa, E. "Autogenous shrinkage of concrete", E & FN Spon, London, UK, 1999, p. 175.

[64] Ravina, D. "Slump Retention of Fly Ash Concrete With and Without Chemical Admixtures", Concrete International, 17(4), pp. 25–29, 1995. [online] Available at: https://www.concrete.org/publications/internationalconcreteabstractsportal/m/details/id/12783 [Accessed: 19 February 2019]